纯铁表面喷丸处理对镍扩散性能的影响

王越田， 盛光敏， 孙建春， 卢 昊
(重庆大学 材料科学与工程学院, 重庆 400030)


王越田

摘 要：采用高能喷丸(HESP)对纯铁棒样端面进行了表面自纳米化(SSNC)处理，通过金相显微镜、扫描电子显微镜及X射线衍射对表面变形层厚度、晶粒度及硬度等进行了表征；然后在Gleeble1500型热模拟试验机上实现镍箔在纯铁表面的渗入，并利用扫描电子显微镜对扩散的效果进行了比较分析．结果表明，工业纯铁经喷丸处理，表面晶粒得到明显细化，表面硬度明显增加，显微硬度比心部基体组织高出近一倍；经过喷丸处理试样表面镍的扩散速率与未经喷丸处理试样相比，有了明显的提高，表面自纳米化技术提高了镍在工业纯铁表面的扩散效果．

关键词：工业纯铁；表面自纳米化；喷丸；扩散
中图分类号：TG178 文献标识码：A 文章编号：0253－360X(2011)05－0021－04

0 序 言

目前，材料表面纳米化的方法主要有表面涂层或沉积、表面自纳米化和混合表面纳米化．其中，表面自纳米化技术因不必考虑纳米层与基体之间的结合，所用设备简单，处理前后构件外形尺寸基本不变，因而具有广阔的应用前景[1]．钢铁材料表面自纳米化是将钢铁材料自身表面层转换成纳米晶结构，同时保持材料的化学组成不变．表面纳米化的原理是采用非平衡处理增加表面层组织的自由能，使晶粒细化，此方法要求在材料表面产生强烈塑性变形或重复形核．目前，主要采用机械处理的方法在材料表面产生强烈塑性变形促使晶粒细化，包括超声机械振动技术、超声喷丸技术、机械研磨、表面轧制、激光喷丸等[2-4]．中科院金属所卢柯研究组采用表面机械研磨(SMAT)的方法已在多种工程材料表面获得了纳米结构层．

纳米化层中的扩渗以及渗层性能的研究也是非常值得关注的问题．为了使纳米化层得到有效的应用，要求其在耐磨、耐蚀和稳定性方面具有优良的综合性能，这些优良性能可以通过渗层技术得已实现[5,6]，而纳米化层由于晶粒细小，具有高体积分数的晶界，能够为原子扩散提供大量通道，大大提高原子的扩散系数[7]．另外，纳米化层中的扩渗元素分布与传统材料可以有极大差别，可以提供非纳米结构不可能获得的特别性能．

文中将表面自纳米化技术运用到扩散中，在短时间内提高了镍在纯铁表面的扩散效果，为后期在纯铁表面实现铬、镍快速共渗打下了基础，使纯铁材料表面改性后表面性能达到或接近不锈钢水平成为可能．

1 试验方法

1.1 试样制备和纳米层表征

试验所用材料为 ϕ10 mm×20 mm的工业纯铁棒样，利用气动喷丸技术对工业纯铁进行表面自纳米化处理，喷丸装置示意图及工作原理如图 1所示．喷丸压力为 0.6 MPa，弹丸直径为 1 mm，喷丸时间为 5 min，喷丸机喷嘴与试样表面的距离都保持在 3～5 cm之间．然后用 X射线衍射仪表征喷丸表面的平均晶粒尺度，测试喷丸试样表面硬度随深度的变化情况．

1.2 纳米纯铁表面镍的扩散及渗层表征

将试样的喷丸面用砂纸磨平，与未喷丸试样的端面对接，中间放置清洁的纯镍箔，其厚度为 13 μm，试样渗镍处理如图 2所示；然后在 GLEEBLE1500型热模拟试验机上进行扩散处理．扩散温度为 850 ℃，升温和降温速度都为 10 ℃/s，脉冲压力为 8～16 MPa，脉冲频率为 0.5 Hz，脉冲次数为 300次(时间为 10 min)．然后用金像显微镜和扫描电子显微镜对接头处镍箔两侧的组织分别进行了观察、比较和分析．

收稿日期：2009－11－25
基金项目：国家自然科学基金资助项目(50675234)

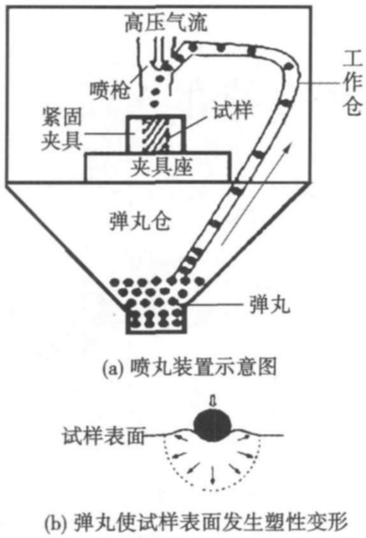

图 1 高能喷丸处理原理图

Fig. 1 Illustration of HESP treatment set-up

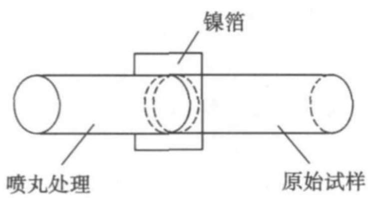

图 2 纳米化前后的试样渗镍处理

Fig. 2 Ni infiltration processing of samples before and after SSNC

2 试验结果及分析

2.1 纳米纯铁的表征

图 3为喷丸面的金相组织形貌, 从图 3中可以看出, 经过喷丸后的工业纯铁表面产生了大量强烈的局部塑性变形, 根据表面纳米化晶粒细化机理得知, 在变形过程中, 表面产生大量缺陷, 如位错、孪晶、层错和剪切带等, 当位错密度增至一定程度时, 发生湮没、重组, 形成具有亚微米或纳米尺度的亚晶, 即图 3中河流状组织.

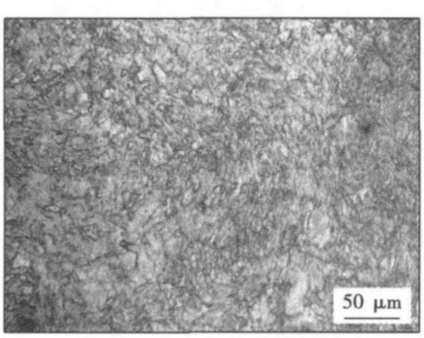

图 3 喷丸面微观组织形貌

Fig. 3 Microstructure of shot peening surface

图 4为喷丸前后试样的 X射线衍射图谱, 从图 4中可以看出, 同原始的粗晶样品相比, 喷丸处理后样品的 X射线 Bragg射线峰明显宽化. Bragg衍射峰宽化是晶粒细化、微观应力增加和仪器宽化 3方面的结果. 考虑不同样品的仪器宽化效应相同, 可见经喷丸处理后, 样品的晶粒尺寸和微观应变发生了明显的变化. 根据 Scherrer-Wilson计算晶粒尺寸方法, 可计算得出喷丸处理后样品表层的平均晶粒尺寸为 43.9 nm[8]. 说明纯铁表面的晶粒已经得到了明显的细化, 最小晶粒尺寸达到纳米级, 从而为后续扩散试验提供了一定厚度的细晶层.

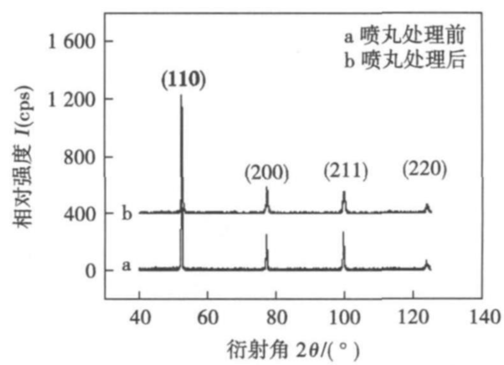

图 4 纯铁的 X射线衍射图谱

Fig. 4 XRD profiles of Fe samples

图 5为喷丸试样纵剖面金相组织形貌, 从图 5中可以看出, 变形层厚度为 130 μm左右, 主要分为表层细晶区、中间晶粒被压扁的过渡区和基体区 3部分, 这是由于弹丸与试样表面碰撞接触的时间很短, 碰撞产生的瞬时应力将以碰撞点为中心向样品的内部传播, 并逐步减小, 因此弹丸每次撞击所产生

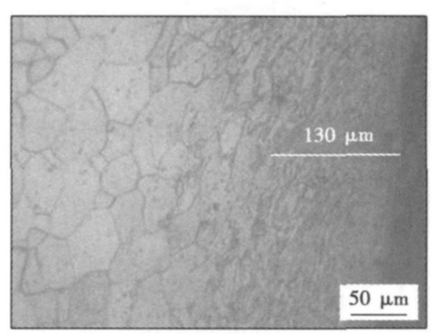

图 5 喷丸试样剖面金相组织形貌

Fig. 5 Cross-section microstructure of shot peening sample

的塑性变形被限制在以碰撞点为中心的局部区域内，试样内部沿着离喷丸表面距离的增加，塑性变形逐步地减弱，并且可能在某个深度达到极值．

图 6为经过喷丸处理试样的显微硬度随距离表面深度变化曲线，从图 6中可以看出，喷丸最表层的显微硬度值为心部基体的近两倍，且硬度在 40 μm的剧烈变形层范围内迅速下降，超过 100 μm后，显微硬度已经趋于基体的硬度．

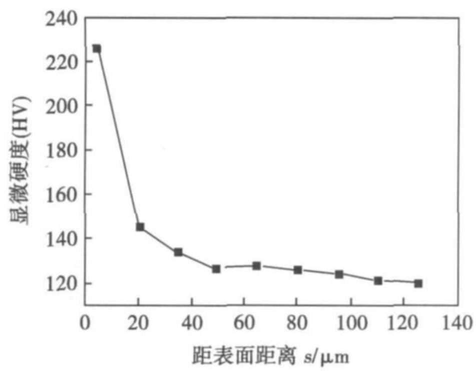

图 6　喷丸试样显微硬度随距离表面深度变化曲线
Fig. 6　Microhardness of shoted sample along depth from top surface

2.2　扩散结果及分析

图 7a为接头处的 SEM形貌，从图 7a中可以看出喷丸一侧试样的晶粒明显的长大了，已经基本接近了基体的晶粒大小，这主要是因为纯铁试样表面在喷丸过程中储存了大量的能量，在高温下晶粒很容易迅速长大；还可以看到在扩散的界面处从镍向纯铁一侧产生了连续的锯齿状的突起．从图 7b中的线扫描图谱可以看出，锯齿状的突起组织是由 Ni元素的聚集所形成，说明镍向纯铁中进行了扩散．由铁—镍相图[9]的分析可知，由于扩散过程升降温速度快，保温温度为 850 ℃，所以可以忽略产生金属间化合物的可能，可以认为铁和镍是无限互溶的．因此，这些突起的组织是以纯镍形式存在，通过退火处理可以使这些 Ni原子分布均匀．

图 8为扩散接头处能谱分析结果，从图 8中可以明显看出镍层左侧含量高于右侧，说明左侧镍向未喷丸处理纯铁的扩散较少，相反，右侧镍向经过喷丸处理纯铁的扩散较多，说明镍向喷丸一侧的纯铁扩散速度较快，体现出了细小晶粒的多晶界对扩散的促进作用．从表 1点扫描结果可以看到，以原始 13 μm厚的镍箔界面为起点，镍实现了向纯铁中的扩散；对比两侧扩散效果，喷丸侧无论是扩散距离还是同一扩散距离的 Ni元素含量均优于未喷丸侧．

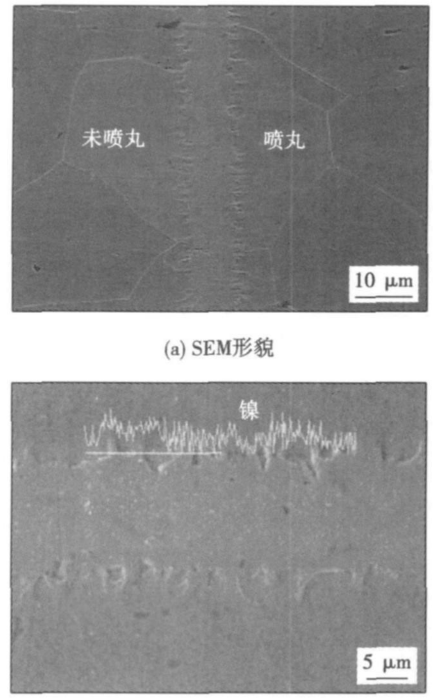

(a) SEM形貌

(b) EDS

图 7　扩散接头处 SEM 形貌和 EDS
Fig. 7　SEM and EDS at diffusion connector

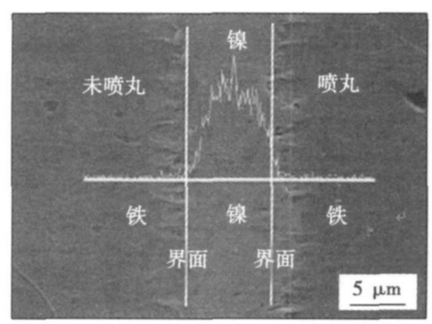

图 8　扩散接头处连续线扫描能谱
Fig. 8　Continuous line scan spectrum at diffusion connector

表 1　扩散接头处点扫描结果（原子分数，%）
Table 1　Spot scanning results at diffusion connector

扩散距离 s/μm	喷丸一侧		未喷丸一侧	
	Fe元素含量	Ni元素含量	Fe元素含量	Ni元素含量
0	30.83	69.17	9.94	90.06
2	68.99	31.01	31.61	68.39
4	73.70	26.30	76.25	23.75
6	91.04	8.96	96.77	3.23
8	97.78	2.22	99.07	0.93
10	99.01	0.99	100.00	—

因此，纯铁经表面喷丸处理提高了镍的扩散速率．

3 结 论

(1)工业纯铁经过 5 min高能喷丸处理,表面晶粒得到极大细化,表层晶粒大小约为 43.9 nm,变形层厚度约为 130 μm.

(2)工业纯铁经过表面自纳米化处理,表面硬度得到显著提高,从表层到心部随着晶粒的增大硬度值下降迅速,直到基体组织的硬度值.

(3)工业纯铁经过高能喷丸处理,在较高的温度下,短时间内明显的提高了镍的扩散效果.

参考文献:

[1] Lu J. Residual stress and mechanical surface treatents: current trends and future prospects[C]// Proceedings of the 4th International Conference on Residual Stress. Baltimore, 1994: 1154-1163.

[2] Liu G, Wang S C, Lou X F, et al. Low carbon steel with nanostructured surface layer induced by high-energy shot peening[J]. Scripta Materialia, 2001, 44(8): 1791-1795.

[3] 李 冬, 陈怀宇, 刘 刚, 等. SS400钢对接接头表面纳米化及其对疲劳强度的影响[J]. 焊接学报, 2001, 23(2): 18-21.
Li Dong, Chen Huaiyu, Liu Gang, et al. Surface nanocrystallization of SS400 steel butt welded joint and its effect on the fatigue strength[J]. Transactions of the China Welding Institution, 2001, 23(2): 18-21.

[4] Wu Ping, Wang Jingyang. Internal frictional elastic study on surface nanocrystallized 304 stainless steel induced by high-energy shot peening[J]. Journal of Materials Science & Technology, 2002, 18(2): 132-134.

[5] 王国阳, 王秀敏, 王德和. 20钢固体粉末法渗硼和硼钒共渗的渗层研究[J]. 金属热处理, 2006, 31(6): 69-71.
Wang Guoyang, Wang Xiumin, Wang Dehe. Study on diffusion layers by solid powder boronizing and borovanadizing process of 20 steel[J]. Metal Heat Treatment, 2006, 31(6): 69-71.

[6] 郝少详, 孙玉福, 杨凯军. Cr12MoV钢渗硼工艺及渗层的组织与性能[J]. 金属热处理, 2006, 31(7): 67-71.
Hao Shaoxiang, Sun Yufu, Yang Kaijun. Microstructure and properties of boronizing layer and boronizing process of Cr12MoV steel[J]. Metal Heat Treatment, 2006, 31(7): 67-71.

[7] Lu K. Nanocrystalline materials crystallized from amorphous solids: nanocrystallization, structure and properties[J]. Materials Science & Engineering R: Reports, 1996, 16(4): 161-221.

[8] Klug H P, Alexander L E. X-ray diffraction procedures for polycrystalline and amorphous materials[M]. New York: Wiley, 1974.

[9] 埃里希, 福克哈德. 不锈钢焊接冶金[M]. 栗卓新, 朱学军, 译. 北京: 化学工业出版社, 2004.

作者简介: 王越田, 男, 1986年出生, 硕士研究生. 主要从事工业纯铁表面改性研究. 发表论文 1篇. Email: wangyuetiansg@163.com

[上接第 20页]

[9] 单际国, 张 婧, 郑世卿, 等. 压铸镁合金激光焊气孔形成原因的实验研究[J]. 金属学报, 2009, 45(8): 1006-1012.
Shan Jiguo, Zhang Jing, Zheng Shiqing, et al. Experimental study on the reason of pore formation in laser welding of die-cast magnesium alloy[J]. Acta Metallurgica Sinica, 2009, 45(8): 1006-1012.

[10] 陈振华, 严红革, 陈吉华, 等. 镁合金[M]. 北京: 化学工业出版社, 2004.

作者简介: 张 婧, 女, 1982年出生, 博士研究生. 主要从事激光焊接方面的研究工作. Email: zhang-jing06@mails.tsinghua.edu.cn

通讯作者: 单际国, 男, 教授, 博士研究生导师. Email: shanjg@tsinghua.edu.cn

100084 China; 2. Key Laboratory for Advanced Materials Processing Technology, The Ministry of Education, Tsinghua University, Beijing 100084, China). p 17—20, 24

Abstract: The effects of welding parameters including laser power, welding speed, welding conditions on pore formation tendency (represented as porosity) during laser welding of die-cast magnesium alloys with two different gas contents were investigated, and the porosity prevention measures were also studied. It is shown that the pore formation tendency during laser welding of 2 mm thick die-cast magnesium alloys with higher gas content is greater than that of 5 mm thick die-cast magnesium alloys with lower gas content. As a whole, the porosity increases with the increase of laser power and the decrease of welding speed for both two thicknesses. For 5 mm thick die-cast magnesium alloys with lower gas content, low porosity weld bead can be obtained by both double sided welding and remelting after welding, and the porosity can reduce to 2.4% and 2.5%, respectively. However, for the 2 mm thick die-cast magnesium alloys, these porosity prevention measures are not effective.

Key words: pore; pore prevention; laser welding; welding parameters; die-cast magnesium alloys

Effect of high-energy shot peening on diffusion behavior of nickel in iron

WANG Yuetian, SHENG Guangmin, SUN Jianchun, LU Hao (School of Materials Science and Engineering, Chongqing University, Chongqing 400030, China). p 21—24

Abstract: High-energy shot peening (HESP) was used to make surface self nano-crystallization (SSNC) on pure iron. The thickness of the deformation layer, surface grain size and hardness were characterized by optical microscope (OM), scanning electron microscopy (SEM) and X-ray diffraction analysis (XRD), and then Ni film was penetrated into the surface of iron by the Gleeble 1500 thermal simulation test machine. The SEM was used to compare the diffusion effects. The results showed that the surface of industrial pure iron was refined obviously after the shot peening treatment, its hardness increased significantly and was one time higher than that of the matrix. Under the same conditions, the diffusion rate of Ni in the specimen after SSNC was higher than that without SSNC, so the SSNC technology can improve diffusion effect of Ni on the surface of industry pure iron.

Key words: pure iron; SSNC; shot peening; diffusion

Signal processing in ultrasonic test of austenitic welds based on time-frequency analysis

WANG Bingfang, HAN Zandong, YUAN Keyi, CHEN Yifang (Key Laboratory for Advanced Materials Processing Technology, The Ministry of Education, Tsinghua University, Beijing 100084, China). p 25—28

Abstract: Signal processing in ultrasonic test of austenitic welds was studied. Based on time-frequency analysis, a comprehensive signal processing method was proposed, which was a combination of matching pursuit and wavelet analysis. This method distinguishes flaw information and material noise from a point of energy and frequency, respectively, and improves the SNR of the ultrasonic echo signal. To verify the effectiveness of the method, an ultrasonic test system was established. Test experiment was carried out with a 53 mm thick weld specimen, and a signal with large amount of material noise was acquired. The noised signal was processed by the proposed method. The first 18 time-frequency atoms were extracted by matching pursuit with sym8 wavelet packet dictionary, the extracted signal was analyzed by sym8 wavelet decomposition and reconstructed with low frequency coefficients. The result shows that the material noise is reduced effectively and the flaw echo signal is enhanced significantly.

Key words: austenitic welds; ultrasonic test; time-frequency analysis; matching pursuit; wavelet analysis

Analysis on growth mechanism on interfacial interlayer on Fe/Al couple

WU Mingfang[1,2], SI Naichao[1], WANG Jing[1], WANG Fengjiang (1. School of Materials Science and Engineering, Jiangsu University, Zhenjiang 212013, China; 2. School of Materials Science and Engineering, Jiangsu University of Science and Technology, Zhenjiang 212003). p 29—32

Abstract: To understand the formation mechanism and growth behavior of Fe-Al intermetallics, the element diffusion and interfacial reactive interlayer in Fe/Al couple were studied at the different heating temperature and holding time. The interfacial structure is Fe/FeAl$_x$ + Al/FeAl/Al at the shorter holding time, while the unstable FeAl$_x$ and FeAl will change into the stable Fe$_2$Al$_5$ and FeAl$_3$ intermetallics at a longer holding time. The final interfacial structure was Fe/Fe$_2$Al$_5$ + FeAl$_3$/Al. The growth of interfacial reactive layer follows the parabolic rule, and its rate is controlled by the diffusion rate of Fe atoms into Al side. The results are helpful to improve the bonding quality between aluminum alloys and stainless steel.

Key words: Fe; Al; diffusion; interfacial structure

Investigation of out-of-plane welding distortion in aluminum alloy welding with external restraint

XIAO Xiaoming[1], PENG Yun[1], ZHANG Jianxun[2], PEI Yi[1], TIAN Zhiling (1. State Key Laboratory of Advanced Steel Processes and Products, Central Iron & Steel Research Institute, Beijing 100081, China; 2. State Key Laboratory for Mechanical Behavior of Materials, Xi'an Jiaotong University, Xi'an 710049, China). p 33—36

Abstract: The characteristics of constraint force and dynamic welding distortion of aluminum alloy 5A12 with constraint TIG welding were investigated by dynamic temperature and distortion measuring system. The effects of constraint force and its release on out-of-plane welding distortion were analyzed. Research results show that out-of-plane welding distortion is different with the different constraint force, and welding distortion can be controlled by the proper constraint force, the welding distortion will rebound to some extent after the constraint force being released, which is the main factor to result in the residual distortion of constraint welding, the residual distortion of 6 mm thick aluminum alloy 5A12 plate can be well restrained at the constraint force of 0.2 kN and the loading position is 45 mm from the centerline of weld.

Key words: aluminum alloy; deformation; constraint force; elastic recovery

Double-pulsed MIG expert database based on mathematical modeling

CHEN Xiaofeng, LIN Fang, WEI Zhonghua, XUE Jiaxiang (School of Mechanical & Automotive Engineering, South China University of Technology, Guangzhou 510640, China). p 37—40